2017

Microfabricated blood vessels undergo neoangiogenesis

Kyle A. DiVito
U.S. Naval Research Laboratory

Michael A. Daniele
North Carolina State University, mdaniel6@ncsu.edu

Steven A. Roberts
U.S. Naval Research Laboratory

Frances S. Ligler
North Carolina State University

Andre A. Adams
U.S. Naval Research Laboratory, andre.adams@nrl.navy.mil

Biomaterials 138 (2017) 142–152

Contents lists available at ScienceDirect

Biomaterials

journal homepage: www.elsevier.com/locate/biomaterials

Microfabricated blood vessels undergo neoangiogenesis

Kyle A. DiVito [a, 1], Michael A. Daniele [b, c, *, 1], Steven A. Roberts [a], Frances S. Ligler [c], André A. Adams [a, *]

[a] Center for Bio/Molecular Science & Engineering, U.S. Naval Research Laboratory, 4555 Overlook Ave. SW, Washington D.C., 20375, United States
[b] Department of Electrical & Computer Engineering, North Carolina State University, 890 Oval Dr., Raleigh, NC 27695, United States
[c] Joint Department of Biomedical Engineering, North Carolina State University and University of North Carolina-Chapel Hill, 911 Oval Dr., Raleigh, NC 27695, United States

ARTICLE INFO

Article history:
Received 15 February 2017
Received in revised form
25 April 2017
Accepted 7 May 2017
Available online 19 May 2017

Keywords:
Sheath-flow microfluidics
Blood vessel
Angiogenesis
Anastomoses
Perfusion

ABSTRACT

The greatest ambition and promise of tissue engineering is to manufacture human organs. Before "made-to-measure" tissues can become a reality [1–3], however, three-dimensional tissues must be reconstructed and characterized. The current inability to manufacture operational vasculature has limited the growth of engineered tissues. Here, free-standing, small diameter blood vessels with organized cell layers that recapitulate normal biological functionality are fabricated using microfluidic technology. Over time in culture, the endothelial cells form a monolayer on the luminal wall and remodel the scaffold with human extracellular matrix proteins. After integration into three-dimensional gels containing fibroblasts, the microvessels sprout and generate extended hollow branches that anastomose with neighboring capillaries to form a network. Both the microfabricated vessels and the extended sprouts support perfusion of fluids and particles. The ability to create cellularized microvessels that can be designed with a diameter of choice, produced by the meter, and undergo angiogenesis and anastomoses will be an extremely valuable tool for vascularization of engineered tissues. To summarize, ultraviolet (UV) photocrosslinkable poly(ethylene glycol) and gelatin methacrylate polymers used in combination with sheath-flow microfluidics allow for the fabrication of small diameter blood vessels which undergo neoangiogenesis as well as other developmental processes associated with normal human blood vessel maturation. Once mature, these vessels can be embedded; perfused; cryogenically stored and respond to stimuli such as chemokines and shear stresses to mimic native human blood vessels. The applications range from tissue-on-chip systems for drug screening, characterization of normal and pathologic processes, and creation and characterization of engineered tissues for organ repair.

Published by Elsevier Ltd.

1. Introduction

Ideally, engineered human blood vessels should possess tunable dimensions and be free standing so that they can be easily handled and integrated into three-dimensional tissues, as well as be connected to perfusion sources. The constructs should also be amenable to storage for later use and self-sustaining in terms of repair and angiogenesis [1–9].

Earlier attempts to produce vasculature for tissue models have used de-cellularized cadaver materials as scaffolds [10], bio-printing of large blood vessels [11], random outgrowth from endothelial cell spheroid cultures or patterned microchannels [12,13]. These approaches have been partially successful, yet fail to provide both the range of microvessel diameters found in normal vasculature and the desired control over microvessel placement within a regenerating tissue [14–18]. A key challenge addressed here is the creation of human vasculature that has not only controllable size and cellular architecture but which can produce new angiogenic growth for long term tissue sustainability, a feature that many other technologies, including 3D printing, have yet to fully realize.

Human vasculature forms through a series of developmental processes. Endothelial sprouting from a main vessel (angiogenesis) launches a network of smaller tubular branches each capable of further sprouting to support blood flow (tubulogenesis). Critical junctions (anastomoses) between arterial and venule capillary beds

* Corresponding authors.
E-mail addresses: mdaniel6@ncsu.edu (M.A. Daniele), andre.adams@nrl.navy.mil (A.A. Adams).
[1] These authors contributed equally to this work.

http://dx.doi.org/10.1016/j.biomaterials.2017.05.012
0142-9612/Published by Elsevier Ltd.

establish a network of arteries/veins, arterioles/venules and capillaries [19]. These three combined processes are essential for tissue maintenance, yet have not been fully replicated in synthetic systems. To date, these processes have largely been accomplished using endothelial spheroid cultures embedded in matrices or pre-patterned microchannels and have not yet been observed from free-standing porous synthetic blood vessels.

The objective of this study is to develop an efficient method of constructing human blood vessels that are both representative and complimentary to microscale human blood vessels. Preferably, these fabricated vessels would then support the formation of a primitive network of blood vessels via the natural processes of angiogenesis, tubulogenesis and anastomosis (Fig. 1), and we sought to characterize the developmental events that occur using our technology. The experimental design begins by creating HEMVs with a desired diameter via hydrodynamic focusing. When seeded into a three-dimensional matrix, the human endothelial microvessels (HEMV) initiate neovascularization which proceeds from angiogenesis through anastomosis. As HEMV technology creates hollow tubular structures with cellular components in place, the ability to immediately perfuse tissue eliminates significant delays associated with tubular development from endothelial networks derived from spheroid cultures. Furthermore, as the HEMV is constructed using a micro-porous [20], biodegradable material, removal of the scaffold is not required. These advantages, together with the possibility for long term storage of HEMV, make the HEMV technology highly useful for *in vitro* tissue engineering and tissue-on-chip analytical systems.

2. Materials and methods

2.1. Fabrication of microvessels

Microvessels were produced using the microfluidic fabrication method previously described [20–22] with minor modifications. Briefly, poly(ethylene glycol) (PEG) tetrathiol and poly (ethylene glycol) acrylate were purchased from JenKem USA (Allen, TX) and resuspended at a 1:1 M ratio in a 1X phosphate buffered saline solution containing 0.4% Irgacure2959 Sigma Aldrich (St. Louis, MO). Gelatin-methacrylamide (GelMA) has been widely identified as a successful substrate for cell attachment in a multitude of bioengineering applications [23,24]. Synthesis of GelMA, using porcine-derived gelatin Sigma Aldrich (St. Louis, MO) was performed as previously described [20] and lyophilized gelatin-methacrylamide was included in the previously mixed PEG polymer also at a 1:1 ratio to provide support for cellular attachment. The final concentration of the mixed polymers is 6% w/w (3% poly(ethylene glycol) and 3% gelatin-methacrylamide). Purified protein components include a mixture of fibronectin (50 μg/mL) from Corning (Bedford, MA), rat-tail collagen-1 (75 μg/mL) and hyaluronic acid (18 μg/mL), both from Sigma Aldrich (St Louis, MO), were added to supplement the poly(ethylene glycol)/gelatin-methacrylamide mixture and further support cellular attachment. The outer sheath fluid is 6% PEG, resuspended in phosphate buffered saline. Cells comprising the lumen are resuspended in a 1% non-photo-crosslinkable gelatin solution; while cells placed in the polymer wall are directly added to the polymer solution. Flow rates for were as follows. Outer sheath 90 μl/min; polymer comprising the microvessel wall 29 μl/min and inner lumen flow is 15 μl/min.

2.2. Microvessel cryopreservation

Day 8 HEMVs were examined for the ability to recover from cryopreservation in three replicate experiments. Briefly, HEMV were removed from the incubator and immediately transferred to cryovials containing endothelial freezing medium (80% EGM-2, 10% fetal bovine serum, 10% dimethyl sulfoxide). Cryovials were then placed into a freezing chamber and transferred to −80 °C overnight.

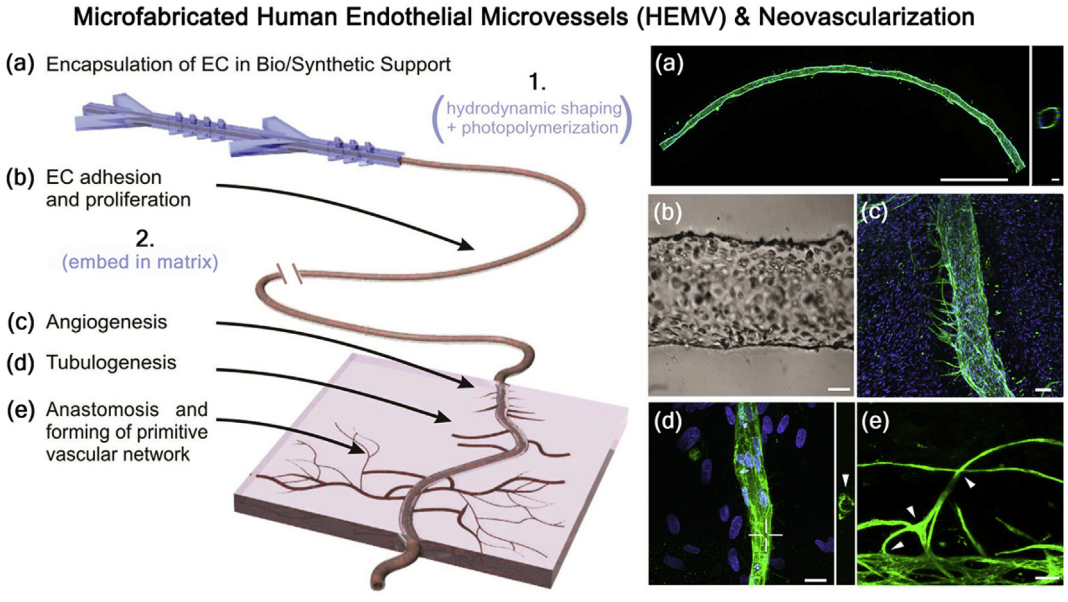

Fig. 1. Neovascularization strategy and implementation. 1. Human endothelial cells (EC) are encapsulated in a bio-macromolecular tubule using a hydrodynamic shaping device. The resultant human endothelial microvessel (HEMV) matures with a coherent endothelial cell lumen. Temporal events a-e (left) correspond to experimental micrographs (right). (a) Representative composite image of ten adjacent fields (10X) taken along the length of a single HEMV immunostained with anti-CD31 (green) demonstrates the ability to produce long continuous HEMVs. Scale, 500 μm; inset 50 μm (b) A confluent monolayer of endothelial cells form along the luminal face of the microvessel. 2. Once embedded in a three-dimensional matrix, the HEMV develop a primitive microvasculature network through traditional vascularization processes, (c) HEMV angiogenesis, the sprouting of endothelial growths from the original HEMV into an extracellular matrix containing dermal fibroblasts (DAPI-stained nuclei, blue), (d) HEMV tubulogenesis (arrowhead), the hollowing of sprouts to support fluid transport, (e) HEMV anastomosis, a developmental process whereby neighboring sprouts form connections (arrowheads) establishing a closed-loop system for circulation. Scale, (b + d) 25 μm; (c + e) 50 μm.

Cryovials were moved to a liquid nitrogen storage dewar and placed into vapor-phase storage for 24 h. HEMV were then thawed at 37 °C and immediately placed into complete growth medium and allowed to recover for 24 h at 37°C/5% CO_2. As a note, suspending HEMV in freezing media and immediately submerging the vial in liquid nitrogen resulted in HEMV structural failure and microvessels were not recoverable. As a positive control for cell death, HEMV were fixed in 10% neutral buffered formalin for 3h and then permeabilized in 1X phosphate buffered saline/0.5% Triton X-100 for 1h, room temp. Cell viability was then examined using Live/Dead® assay ThermoFisher Scientific (Grand Island, NY). 20X images were captured and both live and dead cells were counted and plotted as a ratio of total number of cells. For the inflammatory cytokines assay, native or cryopreserved HEMV were treated with either TNF-α (25 ng/mL) or IL-1β (2.5 ng/mL) EMD Millipore (Billerica, MA) for up to 4 h. Cryopreservation was performed as reported above, with cytokine treatment performed on fully recovered HEMV and done in parallel with native microvessels. Real-time quantitative PCR was then used to assay the expression of the P– and E-selectin genes; with GAPDH as control. The statistical analyses depicted (ANOVA) compare each time point to the matched untreated (0 h) control.

2.3. Cell/vascularization experiments

2.3.1. Human cells and growth media

Primary human umbilical vein endothelial cells and primary human dermal fibroblasts were obtained from Lonza (Walkersville, MD) and passaged as recommended. Endothelial growth medium-2 with required supplements (Lonza) was used to grow endothelial cells; while fibroblasts were cultured in DMEM plus 10% fetal bovine serum ThermoFisher Scientific (Waltham, MA). Human primary vascular smooth muscle cells were obtained from ATCC (Manassas, VA) and grown in DMEM/F12 (1:1) with 10% fetal bovine serum plus endothelial growth factor supplement (Sigma), along with the buffers sodium selenite, sodium bicarbonate as recommended. Human vascular pericytes were obtained from ScienCell (Carlsbad, CA) and grown in DMEM/F12 growth medium containing 10% fetal bovine serum. All cells were maintained at 37 °C in 5% CO_2 and not used for experimentation beyond passage five. Cells were deemed negative for mycoplasma contamination using MycoProbe R&D Systems (Minneapolis, MN). For microvessel construction, 3×10^7/mL endothelial cells were used to form the lumen of both single- and multi-cell microvessels; 5×10^6/mL smooth muscle cells and pericytes were grown in separate cultures and then combined (1:1 ratio) to form the multi-cell microvessels. Multi-cell microvessels containing HUVEC/SMC/HVP were maintained in 50% composite growth media containing 50% EGM2 (Lonza) and 50% DMEM/F12 10%FBS as both SMC and HVP were maintained using this medium.

2.3.2. Antibodies

Monoclonal anti-CD31 (Ab-1) was obtained from ThermoFisher (Waltham, MA) and used at a 1:200 dilution; anti-VE-cadherin was obtained from Santa-Cruz Biotechnology (Dallas, TX). Secondary antibodies were Alexa-488 and Alexa-594 and used at 1:1000 Life Technologies (Grand Island, NY). Anti-collagen IV (clone COL-94) was used at 1:500; anti-laminin was used at 1:100; anti-collagen VII (LH7.2) was used at 1:500, all were obtained from Sigma Aldrich (St. Louis, MO). Anti-porcine-specific collagen I/III (C7510-18Q) was used at 1:25 as recommended by manufacturer USBiological (Salem, MA). Phosphorylated-Smad2 ($Ser^{465/467}$)/Smad3 ($Ser^{423/425}$) (clone D27F4) was obtained from Cell Signaling Technologies (Danvers, MA). Anti-Ki-67 (clone 35) was obtained from BD Biosciences (San Jose, CA). Anti-alpha-smooth muscle actin (α-SMA; PA5-16697) was obtained from ThermoScientific. Neural glial antigen-2 (NG2) was obtained from Millipore (Billerica, MA) and used at 1:100 as recommended. Anti-E-selectin (clone 1.2B6) was obtained from ThermoFisher (Waltham, MA) and was used at 2 μg/mL.

2.3.3. Confocal microscopy/fluorescence quantitation

Image capture was performed using a Nikon laser scanning confocal microscope; Nikon Elements and Adobe Photoshop software were used for image rendering. At least five representative regions of interest were captured over each triplicate experiment and used for quantitative analyses using mean fluorescence intensity determined using ImageJ (NIH) as previously reported [25,26]. Images of secondary-only negative controls were also collected and used for the purposes of background fluorescence quantitation.

2.3.4. Angiogenesis assays/immunofluorescence

HEMVs were constructed and placed in a CO_2 incubator for 7 days to allow attachment/growth of endothelial cells to the inner luminal face of microvessel. Primary dermal fibroblasts have been shown to facilitate angiogenesis [27,28]. Therefore, fibroblasts were trypsinized, collected and counted and resuspended at 5×10^5 cells/mL in the hydrogel solutions described below. Using surgical forceps and scissors, microvessels were first cut into shorter lengths then transferred to either 24-well cell culture plates or glass coverslips (coverslips were used for high magnification confocal imaging). Microvessels were then overlaid with solutions of either 4% gelatin-methacrylamide/0.5% photoinitiator (PI) or growth factor reduced Matrigel® BD Biosciences (San Jose, CA) containing primary fibroblasts, plus recombinant human vascular endothelial growth factor (rhVEGF, 60 ng/mL) and basic fibroblast growth factor (bFGF, 30 ng/mL). Gelatin-methacrylamide was photopolymerized with UV light (10 mW/cm^{-2}, 5 s); Matrigel® was allowed to cure at 37 °C for 1hr. Four individual microvessels were used in three separate experiments; the results presented are representative of the biological replicates. Cell-laden microvessels were maintained in growth media and were harvested after 17–21 days unless otherwise indicated; growth media was replaced with fresh media every other day. The above protocol was replicated for HEMV tissue constructs lacking dermal fibroblasts. At the end of the growth period, microvessels were fixed in 4% neutral buffered formalin for 1hr, on ice, followed by permeabilization in 1X phosphate buffered saline/0.5% TritonX-100 for 30 min, on ice. Immunofluorescence was performed as previously reported [25]. Briefly, pre-diluted primary antibody was added to the microvessels and incubated overnight, 4 °C. The following day, microvessels were washed 3X in phosphate buffered saline containing 0.05% Tween-20 (PBS-T) and then incubated in secondary antibody for 3 h at room temperature. Finally, DAPI was added at the end of the incubation period for 5 min, and microvessels were extensively washed in PBS-T.

Transforming growth factor-beta (TGF-β) is a critical signaling pathway involved in angiogenesis [29]. Therefore, the ability of the TGF-beta pathway to become activated in the HEMV was addressed using purified TGF-beta growth factor. HEMV were serum starved overnight and the following day 5 ng/mL recombinant human TGF-β R&D Systems (Minneapolis, MN) was added to HEMV for 10min. HEMV were then fixed and stained for *p*-Smad2/3.

Neural glial antigen-2 (NG2) has been previously shown to identify human pericytes at least initially, however in the presence of other cell types such as smooth muscle cells (SMC), pericytes can readily transdifferentiate into SMC [30–33]. To address neural glial antigen-2 (NG2) expression over time, 100×10^3 human vascular pericytes (HVP) were plated at confluency into 24-well plates and

maintained either as a mono- or co-culture with smooth muscle cells (SMC). For co-culture, HVP and SMC were mixed at a 1:1 ratio and cultured over a 7 day time course, with daily media changes. Cells from day 1 and day 7 were then fixed in 4% neutral buffered formalin and immunostained simultaneously using either anti-NG2 or anti-α-SMA overnight at 4 °C. Five separate 20X images, representing >500 cells were captured for each condition and mean fluorescence intensity was determined using ImageJ (NIH) after normalizing to cell number. The mean fluorescence intensity for NG2 or α-SMA was then plotted for both the mono- or co-culture conditions.

2.4. Microvessel cannulation/perfusion experiments

Microvessel perfusion was executed using either of two approaches. For the cannulation experiments, three HEMVs were placed onto separate glass coverslips and, microvessels were overlaid with 4 % gelatin-methacrylamide/0.5 % Igracure-2959 and photopolymerized to immobilize while leaving both termini exposed for cannulation and flow-through. Polycarbonate microcapillaries with dimensions of 80 μm OD/53 μm ID Paradigm Optics (Vancouver, WA) were then manually threaded into the microvessel with the aid of a dissecting microscope while keeping the microvessel hydrated in phosphate buffered saline. Connections were made via threading the capillary into a Luer-Lok tip attached to a 1 mL syringe; the syringe was then loaded into a syringe pump Harvard Apparatus (Holliston, MA). Once the microvessel was cannulated, perfusion was initiated in a stop-flow fashion using a 1 μL/min flow rate; flow was permitted for approximately 2 min. For cannulation experiments, fluorescent Nile Red microparticles (NRμp, 0.52 μm OD) SpheroTech (Lake Forest, IL) were used at 1:100 in 1X phosphate buffered saline. Microvessels were then imaged using confocal microscopy. For perfusion of live cell-laden microvessels, a novel manifold device was constructed by casting polydimethylsiloxane (PDMS) into micro-milled aluminum molds. Once cured, the device was then delaminated, microvessels were removed from the CO_2 incubator and placed in between polydimethylsiloxane pillars of the mold designed to hold the microvessels in place under perfusion. For sealing the devices, a 2 × 3 inch glass slide Fisher (Pittsburgh, PA) and the polydimethylsiloxane device were plasma coated using a hand-held corona treater from Electro-Technic Products (Chicago, IL) and immediately sealed. The center cavity of the device was filled with 4% gelatin-methacrylamide/0.5% photoinitiator through existing biopsy punches present on the device; gelatin-methacrylamide was then photopolymerized. Inlet cavities were then perfused with endothelial growth media via a micro-peristaltic pump; mediate was recirculated by collecting perfusate from the outlet present on the device. Flow was introduced at 3.1 μL/min, which corresponds to a shear rate of 4.2 dyn/cm^2 of observed shear stress. Manifold devices were transferred to a 37°C/5% CO_2 incubator to maintain cell viability; growth media was also placed into the incubator and left uncapped to permit gas exchange. Perfusion fluids continually recirculated for the times indicated.

2.5. COMSOL simulations

Simulations for shear rate and shear flow were performed using finite-element analysis software COMSOL Multiphysics® (Burlington, MA). Cylindrical models with an extra fine mesh density and diameters of 125 and 100 μm were used as a representation of the microvessel lumen. The parameters for viscosity and density were set at 7.8×10^{-4} Pa s and 1007 kg/m^3, respectively [34]. Calculations for shear rate were carried out for flow rates ranging from 20 μL/min to 0.5 μL/min.

2.6. Quantitative RT-PCR

Total RNA was collected from four individually perfused microvessels in each of three separate experiments by dismantling the polydimethylsiloxane device, harvesting the embedded microvessels and transferring to TRIzol® reagent Life Technologies (Grand Island, NY). Real-time PCR was performed using a two-step method. RNA was quantitated via NanoDrop™ and 175 μg of total RNA was used for first strand cDNA synthesis via SuperScript IV, which was followed by real-time PCR performed using Power SYBR™ Green master mix, both Life Technologies (Grand Island, NY). Quantitative PCR was performed using an Applied Biosystems instrument (Carlsbad, CA). Analyses of RT-PCR data was performed using the delta-delta Ct method following amplification efficiency analysis using 10-fold dilutions of template cDNA, as previously described [25]. Custom oligos were purchased from Eurofins Genomics (Huntsville, AL). A list of corresponding oligo sequences can be found in Table S1.

2.7. Statistics

All plots, normality testing and statistical analyses were generated using OriginPro 8.5 OriginLab Corporation (Northampton, MA). Asterisks represent results from either two-sided Student's *t*-test, or ANOVA along with Tukey post-hoc means comparison, where $^*p < 0.05$; $^{**}p < 0.01$; $^{***}p < 0.001$.

2.8. Data in brief

Data describing media compatibility experiments for all the relevant cell types, the denuding of the polymeric shell of the microvessel and information regarding microvessel composition and construction have been submitted as a *Data in Brief* article [35].

3. Results and discussion

3.1. HEMV fabrication and characterization

The HEMV microfabrication process uses hydrodynamic focusing to surround a continuous flow of suspended cells with a biocompatible hydrogel network [20,36,37]. This fabrication process (Fig. S1) incorporates single or multiple cell types into discrete regions of the microvessel during assembly. The length of HEMV produced is limited only by the volume of source materials and, in this study, continuous production of greater than 1 m of HEMV with an inner diameter (I.D.) of 125 μm is obtained in each experimental run. The hydrodynamic focusing technique also facilitates HEMV dimensional tuning by controlling fluid flow rates [20]. In consideration for potential clinical and translational applications, an outer diameter (O.D.) of 250 μm was selected to obviate the need for specialized handling tools during manipulation.

Human umbilical vein endothelial cells are introduced in the lumen of the HEMV during fabrication; cellular attachment to the luminal wall is observed after 3 days. Cell expansion continues until a confluent monolayer is apparent by day 10 (Fig. 2a). Arterioles contain multiple cell types and are modeled by introducing vascular smooth muscle cells and pericytes into the wall of the microvessel during the fabrication process and are referred to as multi-cell microvessels (MCMV). The endothelial cells line the lumen, while smooth muscle cells proliferate to fill the abluminal wall by days 7–10, with continual growth through days 15–20 (Fig. 2a; Fig. S2) and beyond.

Characterization of the HEMV with laser-scanning confocal immunofluorescence microscopy (LSCM) determines the expression and localization of biomarker proteins in HEMV at various time

points. Cells in the luminal wall of the HEMV expressed the endothelial biomarker CD31 and vascular endothelial-cadherin (VE-cadherin) (Fig. 2b and Videos S1, S2). For MCMV, media compatibility assays determined the composite growth media required to support each cell type and a 50/50 composite formulation was used for experimentation, these data can be found in our companion paper [35]. Immunofluorescence staining identifies the cell types incorporated into the MCMV (Fig. S2a). Alpha-smooth muscle actin (α-SMA) is expressed by both smooth muscle cells (SMC) and pericytes, while neural glial antigen-2 (NG2) has been shown to identify pericytes. Yet, both of these cell types are closely linked and transdifferentiation of pericytes into smooth muscle cells has been observed making cell fate tracking difficult [30,38–41]. Using an *in vitro* co-culture assay, we address biomarker expression over time (Fig. S2b) and find that NG2 expression, while a viable marker for pericytes in mono-culture, was reduced after 24 h and further reduced by up to 2.5-fold ($p < 0.01$) day 7 in co-culture with smooth muscle cells, indicating that NG2 expression is likely not suitable to distinguish pericytes from the smooth muscle cells used to create the MCMV. Nevertheless, this multi-compartmental strategy enables the placement of multiple cell types into the microvessel without disrupting the structural integrity of the MCMV during initial cell expansion.

Supplementary video related to this article can be found at http://dx.doi.org/10.1016/j.biomaterials.2017.05.012.

Downstream applications such as *in vitro* tissue constructs require *de novo* synthesis of human derived proteins. Therefore, the time-dependent deposition of extracellular matrix proteins including collagens IV, VII and laminin were evaluated. Twelve days after fabrication (T0), striking expression of both human collagen IV (6.5-fold; $p < 0.001$) and human laminin (>13-fold; $p < 0.001$) were observed in the walls of the HEMV (Fig. 2c and d). As a control, skin-associated [42] collagen VII was assayed and found undetectable at T0 and day 12 (Fig. S3a). Further, a significant decrease (>2-fold; $p < 0.001$) in the porcine-derived collagen I/III, originally included in the HEMV scaffold, was observed after 30 days, when compared to T0 (Fig. S3b).

VE-cadherin is a critical biomarker integral for the long-term maintenance of microvessels. Expression of VE-cadherin identifies adherens junction formation in the HEMV by day 10, with persistent expression through day 120 (Fig. 3a). Further, HEMV maintain their hollow tube morphology (Figs. 2b and 3a), a feature indispensable for proper vascular perfusion. Taken together, VE-cadherin indicates cells establish proper cell-cell junctions; while *de novo* human collagen IV and laminin accumulation, along with reduced porcine-derived collagen, indicate resident cell populations of the HEMV progressively remodel their environment by depositing matrix proteins and replacing exogenous materials. Remodeling of the surrounding matrix is essential for promoting structural integrity, initiating angiogenesis and subsequent vascular expansion.

3.2. HEMV preservation and response to biological cues

Reliable HEMV fabrication and storage could enable a transition toward rapid manufacturing of vascularized tissue constructs. Recently, induced pluripotent stem cell (iPSC) technology has successfully differentiated endothelial cells from dermal fibroblasts [2]. As demand for personalized medicine increases, tailored-HEMV could be prospectively constructed and banked for future use via an iPSC source. To that end, cryopreserved HEMV was evaluated

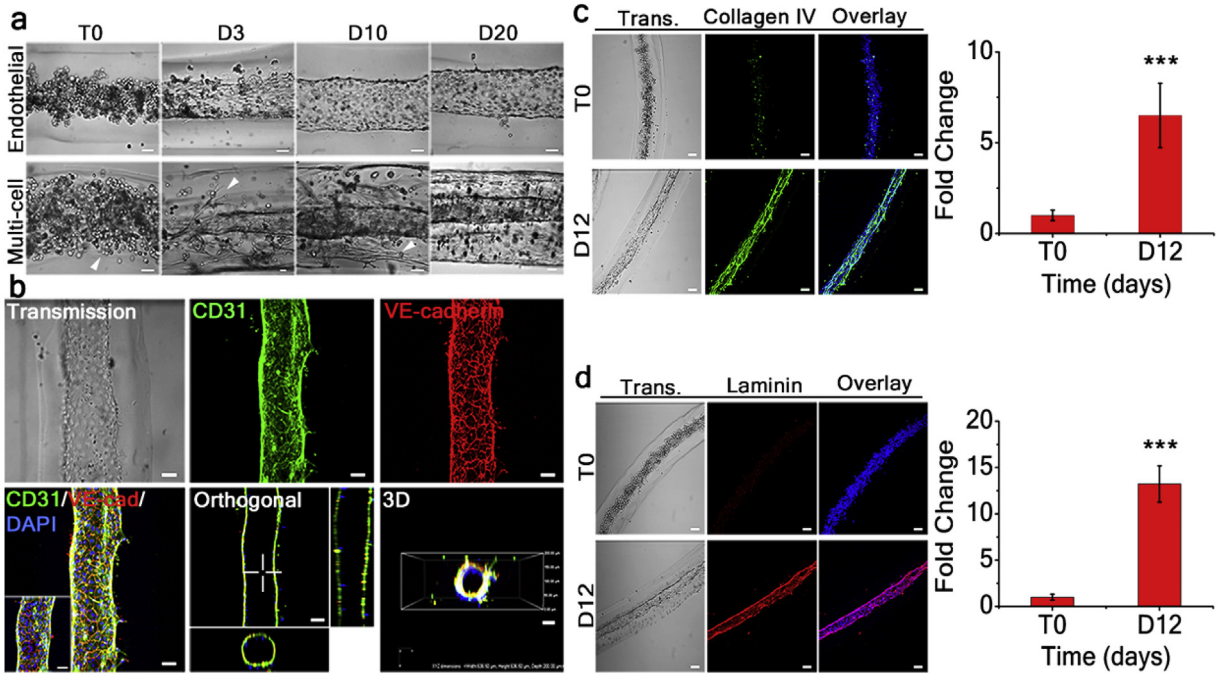

Fig. 2. Characterization of cell-laden HEMV. (a) *Top*, depicts a 20-day time course showing endothelial cell attachment to the inner luminal face of the HEMV, forming vessel mimics similar in size and cellularity to capillaries and venules. *Lower*, multi-cell microvessel composed of endothelial cells (lumen) and smooth muscle cells/pericytes (outer-walls) creates an arteriole-like mimic. Scale, 50 μm. Arrowheads depicts smooth muscle cell/pericyte placement and outgrowth in walls. (b) Laser scanning confocal microscopy identifies cell surface protein expression in day 12 HEMV. Endothelial cells express both CD31 (green) and VE-cadherin (red), confirming the cell type and the presence of critical adherens junctions necessary for proper endothelial function. CD31 (green); VE-cadherin (red); DAPI (blue nuclear stain) overlay is also shown. Both orthogonal and 3D views confirm the hollow, tubule morphology of the created HEMV. Scale, 50 μm (c and d) Anti-collagen IV and anti-laminin show accumulation of newly secreted human matrix protein. Top panels show representative HEMV at time zero (T0); bottom panel shows microvessels analyzed at day 12. Day 12 HEVM were observed with a 6.5-fold increase in collagen IV ($p < 0.001$); similarly laminin exhibited a 13-fold increase in expression ($p < 0.001$) when compared to T0 microvessels. Scale, 100 μm.

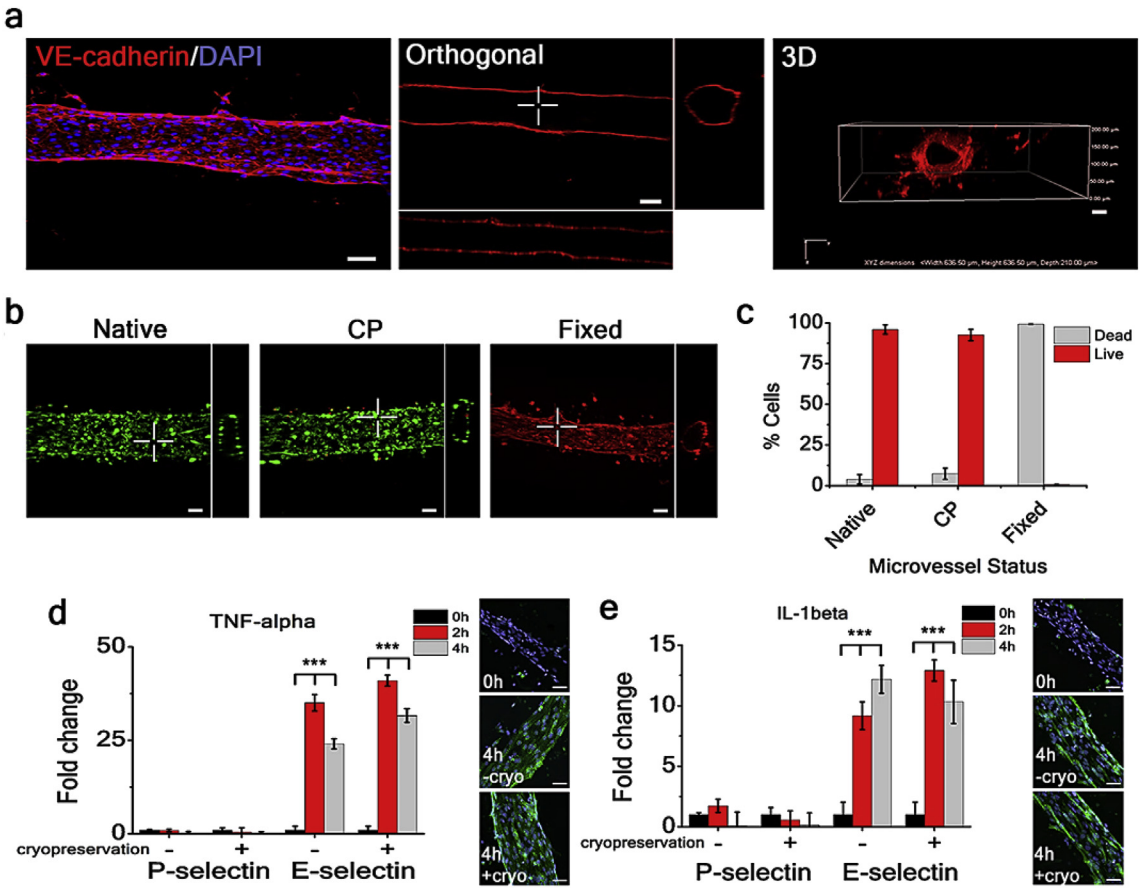

Fig. 3. Long-term HEMV viability, cryopreservation and response to inflammation. (a) Representative HEMV grown for 120 days in growth-media suspension and immunostained with anti-VE-cadherin (red); DAPI (blue) identifies nuclei. VE-cadherin is expressed at the cell surface and structural integrity of microvessel is maintained as shown via 3D confocal images. In addition, small endothelial sprouts can be observed at the periphery of the lumen, indicating potential neoangiogenesis while in suspension. Scale, 50 μm (b and c) Live/dead assay performed on native, cryopreserved (CP), or formalin-fixed HEMV (day 8). Live cells (green); dead cells (red). Insets to the right of each image show orthogonal images depicting the hollow structure of representative HEMV for each condition. No statistical change in percentage of dead cells was observed following recovery from cryopreservation. Scale, 50 μm (d and e) To assess the ability of HEMV to respond to inflammatory signals, native (−) or cryopreserved (+) HEMV were treated with either tumor necrosis factor-alpha (TNF-alpha) or interleukin-1beta (IL-1beta) for the indicated times. Real-time PCR identifies up to a 40-fold increase ($p < 0.001$) in E-selectin gene expression following TNF-alpha treatment and, similarly, up to a 12-fold increase ($p < 0.001$) following IL-1beta treatment. Statistical assessments shown compare experimental (2h, 4h) to matched (0h) untreated control. Adjacent immunofluorescence images depict increased expression of E-selectin (green) following the respective treatment. DAPI (blue) Scale, 50 μm.

initially for cell viability and subsequently for the ability of the recovered constructs to exhibit normal endothelial cell functions (Fig. 3b–c). Live/dead staining reveals no statistical change in percentage of dead cells following recovery from cryopreservation.

A critical aspect of functional vasculature is response to inflammatory signals delivered to endothelial cells via circulating inflammatory cytokines [43]. To further characterize the HEMV technology, a response to inflammation assay was measured using quantitative-PCR on both native and cryopreserved day 8 HEMV (Fig. 3d–e). Cytokines such as tumor necrosis factor-alpha (TNF-α) and interlukin-1beta (IL-1β) are critical pro-inflammatory signaling molecules responsible for triggering endothelial expression of leukocyte adhesion genes such as E-selectin. Native or cryopreserved HEMV treated with either TNF-α or IL-1β increased E-selectin production up to a 40-fold increase ($p < 0.001$) and up to a 12-fold increase ($p < 0.001$), respectively, when compared to untreated control HEMV. In most cases, E-selectin was strongly elevated 2 h post treatment with reduced expression observed by 4 h. The observed expression was evident either in the presence or absence of cryopreservation; the only statistical significance between those groups was identified following IL-1β (2 h) treatment, where the cryopreserved group indicated a slightly more potent E-selectin response ($p < 0.01$) compared to the native HEMV (2 h). The observed effects are consistent within time frames and concentrations reported for human endothelial cells [44–47]. A similar upregulation of E-selectin protein is exhibited following treatment with TNF-α or IL-1β. P-selectin preferentially responds to the clotting factor thrombin [47,48] and was not induced over the time course assayed and serves as a negative control. These data provide not only functional assessment regarding gene expression in HEMVs following cryopreservation, but also provide valuable information regarding the ability of both native and cryopreserved HEMV to stimulate genes necessary for leukocyte attachment in response to inflammatory signals.

Endothelial cell proliferation and cell-signaling pathway activation were also assayed to determine if cells in HEMV recapitulate normal cellular functions. To address primary cell proliferation and quiescence following cell integration, the Ki-67 nuclear proliferation marker was assayed. At time zero (T0), >70% of resident endothelial cells are actively undergoing replication evidenced by nuclear expression of Ki-67. The Ki-67 expression is coupled with minimal cell-surface expression of VE-cadherin (Fig. S4a), indicating that the endothelial cells have not yet exhibited contact inhibition. Once continuous cell-cell contacts are established, Ki-67 expression is reduced 3.5-fold ($p < 0.001$) and a concomitant potent increase in VE-cadherin is observed at the homotypic cell-cell

junctions. This pattern is consistent with the process whereby normal mammalian cells undergo contact inhibition and enter a reversible phase of the cell-cycle (quiescence) to avoid over proliferation.

Furthermore, to validate that cells in the HEMV recapitulate other normal functions, we interrogated the transforming growth factor-beta (TGF-β) signaling pathway as it is directly involved in angiogenesis [29]. Activation of the TGF-β pathway via the surrogate marker phosphorylated-Smad2/3 [49] indicates TGF-β-treated HEMV strongly induces Smad2/3 phosphorylation, resulting in nuclear retention (Fig. S4b). Consequently, cells present in the HEMV proliferate until confluent, establish cell-cell adherens junctions and activate signaling pathways, which are three significant indicators of a biologically functional blood vessel.

3.3. Neoangiogenesis

In the absence of angiogenic potential, incorporation of vasculature alone is insufficient to support complex tissue as simple diffusion is inadequate for nutrient transport beyond 1 mm [50,51]. Therefore, organized endothelial expansion beyond the primary HEMV is necessary to sustain three-dimensional tissue constructs. We hypothesized that denuding the biopolymeric shell of the HEMV might be required for neoangiogenesis and we successfully denuded day 7 HEMV via collagenase digestion or mechanical disruption [35].

However, further examination of intact HEMV revealed short protrusions extending into the surrounding biopolymeric shell (Fig. 3a), which suggested that resident endothelial cells could undergo angiogenic sprouting through the synthetic microvessel wall. Further studies thus focused on supporting the angiogenic potential of the intact HEMV by embedding them in a hydrogel containing normal human dermal fibroblasts to mimic a tissue environment. Endothelial cell-only HEMV provided the opportunity to characterize endothelial expansion and endothelial sprouts easily distinguished from the fibroblasts present in the surrounding gel. Under these conditions substantial endothelial sprouting (Fig. 4a–c) was observed when embedding intact HEMV in the presence of primary fibroblasts.

Two different types of hydrogel, both containing dermal fibroblasts, were investigated for incorporation of the HEMV into a model tissue. Growth-factor-reduced Matrigel® or 4% gelatin-methacrylamide both supported endothelial expansion from the HEMV with no marked difference observed in overall sprouting performance. Matrigel® slightly increased the average number of endothelial sprouts, though this did not reach statistical significance ($p > 0.59$). Thus, while maintaining microvessel integrity after removing the polymer walls is feasible [35], it is not required as the HEMV clearly exhibit prolific neovascularization using as-fabricated microvessels.

Further, embedded HEMV retain the hollow-tubule morphology, indicating HEMV structural stability (Fig. 4a). Dimensionally, sprouts are wider closest to the microvessel and narrow to <8 μm in width at sprout termini. Sprout lengths measured from the outer edge of the HEMV to the advancing tip ranged from 50 μm to 1290 μm (Fig. 4c) with a median length of 547 μm; shorter assay times resulted in shorter overall lengths, indicating that 1.3 mm may not be the upper limit of growth. Remarkably, endothelial sprouts were also observed to traverse the synthetic wall of the HEMV (Fig. 4a; Figs. S5a–d), a critical feature essential for vascularization and ultimate tissue integration. Furthermore, observed interactions between neighboring embedded HEMVs, via capillary outgrowth, indicates putative HEMV-HEMV linkages (Fig. S5d).

Having observed HEMV neoangiogenesis, we next verified that the newly-formed sprouts were hollow tubules. Fig. 4d (center) depicts a representative $CD31^+$ angiogenic sprout, while flanking insets show representative high-magnification images. Orthogonal laser scanning micrographs confirm the hollow nature of the sprouts with an average luminal diameter of 4±1 μm. Extensive $CD31^+$ filiopodial projections are observed along the lengths of many sprouts and are indicative of continued endothelial expansion (Fig. 1d; 4d-e). Anastomoses among angiogenic sprouts were virtually innumerable (Fig. 4e), pointing toward terminal development of a complex vascular network. Further, fibroblasts play an integral role in angiogenesis by providing matrix remodeling necessary for endothelial outgrowth, and organized DAPI-labeled fibroblasts were observed upstream of the advancing $CD31^+$ bifurcated endothelial tip (Fig. S5c), results consistent with previous observations [27,28].

The growth status and efficacy of dermal fibroblasts included in the extracellular matrix of HEMV tissue constructs was also assessed. Similar to CD31, we find VE-cadherin expression is maintained on endothelial sprouts derived from HEMV embedded in a fibroblast matrix (Fig. S6a) indicating sprouts support cell-cell adhesions. Using Alexa488-phalloidin to identify cytoskeletal F-actin, embedded fibroblasts display a spheroidal morphology at time zero, as expected. By day 5, fibroblasts present in the hydrogel display characteristic bipolar, elongated morphology consistent with viable fibroblast expansion (Fig. S6b) [52]. When fibroblasts were excluded, endothelial sprouting was found to be significantly reduced with only short projections of 27 μm median length observed nearest the HEMV lumen at the time of collection on day 21 (Fig. S6c). In the absence of fibroblasts, $CD31^+$ endothelial sprouts failed to exit the polymer wall of the HEMV by the time point assayed, indicating that fibroblasts were integral to the development and maturation of endothelial sprouting derived from the HEMV.

3.4. HEMV perfusion and shear stress response

To investigate whether sprouts support perfusion, embedded HEMV were cannulated using polycarbonate capillaries (Fig. S7). The HEMV remained viable under approximate pressures of 150–2500 Pa without failure and were able to withstand shear stresses up to the flow-rate limits of the peristaltic pump (25 dyn/cm^2). Three distinct regions of interest are used to illustrate perfusion (Fig. S7b). Insets show that NRμp enter newly formed sprouts, confirming the HEMV are hollow and support fluid transport. However, not all angiogenic sprouts were identical (Fig. S7c); NRμp are present in the lumen of $CD31^+$ positive endothelial sprouts but absent in immature or otherwise occluded sprouts, with NRμp exclusion likely due to ongoing sprout development, as has been previously observed [53,54]. On average, mature sprouts supporting perfusion were found to outnumber immature sprouts by a ratio of 3:1.

Finally, shear stress was investigated to validate the HEMV method of neovascularization (Fig. S8; Videos S3a and b) using both experimentally derived observations as well as COMSOL simulations. Not only does shear stress generate forces that act upon the vessel, but cells undergo morphological changes in response to pulsatile perfusion. Therefore, to illustrate that HEMV support perfusion in a microvessel containing living cells, a novel manifold device [52,55] in conjunction with a peristaltic pump was used to recirculate either growth media or Nile Red microparticles through individual microvessels.

Supplementary video related to this article can be found at http://dx.doi.org/10.1016/j.biomaterials.2017.05.012.

Genes related to shear stress have been widely investigated, in more rigid models, with links to multiple cell signaling pathways,

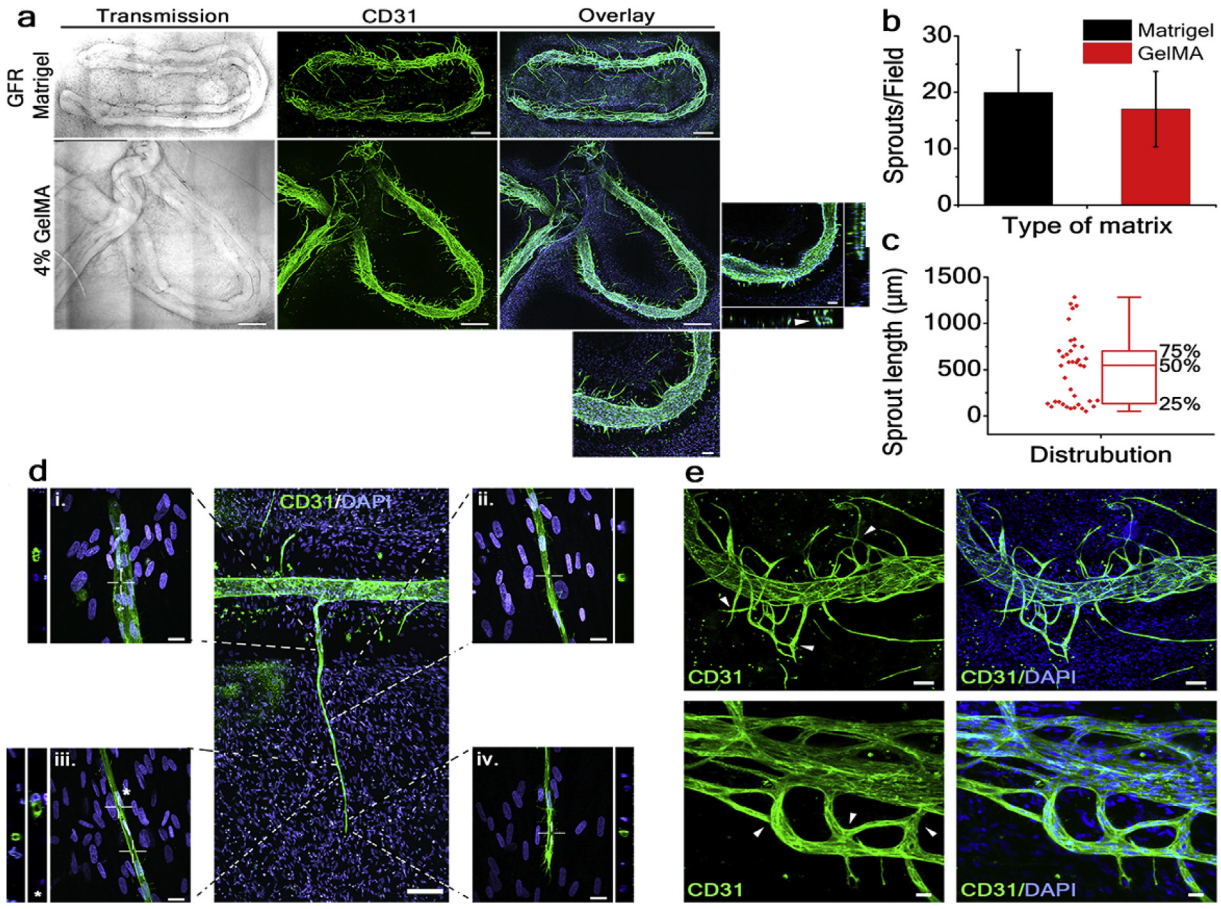

Fig. 4. HEMV undergoing neovascularization. (a–c) Day 17 panoramic images (10X) of representative embedded HEMV showing angiogenic sprouting throughout fibroblasts matrices (DAPI). Both GFR-Matrigel® and 4%-GelMA support angiogenesis. Lower right micrograph, 20X confocal orthogonal views showing HEMV remain hollow (arrowhead) during angiogenic growth. Scale, 500 μm; inset 50 μm. (b) No statistical difference ($p > 0.59$) between the matrices was observed when comparing the number of naïve sprouts present/10X field. (c) Sprout lengths from four individual GFR-Matrigel® embedded HEMV were quantified. Lengths varied from 50 to 1290 μm, with a median of 547 μm after 21 days. $n = 38$ (d) Depicts a panoramic image focusing on a single sprout (center) stained with anti-CD31 (green) and DAPI (blue). Four separate positions along the microvessel (60X) are also shown. Adjacent orthogonal views show the hollow nature of the sprouts. Inset iii, denoted with an asterisk, shows the displacement of a sprout nucleus to the outer edge of the sprout. Close inspection of anti-CD31 reveals extensive filopodial projections, indicating continual expansion through 21 days. Scale, 200 μm; inset 25 μm. (e) Upper (10X) and lower panels (20X) show representative HEMV undergoing neovascularization. Arrowheads depict multiple anastomoses, whereby a single sprout connects with a neighboring growth. Overlaid images anti-CD31 (green) and DAPI (blue) are shown right. Scale, 50 μm (10X); 25 μm (20X).

including TGF-β [56]. TGF-β itself has pervasive effects upon cellular growth dynamics and can effect proliferation, differentiation, migration and blood vessel maturation. TGF-β stimulates various response genes called Smads that either propagate or inhibit the TGF-β signal. Smad6 and Smad7 are inhibitory-Smads (I-Smads). Smad6 limits the signaling of the bone morphogenetic protein (BMP) receptor, while Smad7 predominantly inhibits TGF-β [57–59]. Changes in expression of other genes such as Krüppel-like factor-2 (KLF2); chemokine receptor-4 (CXCR-4); sphingosine kinase-1 (SPHK1); sphigosine-1-phosphate phosphatase-1 (SGPP1); and sphingosine-1-phosphate lyase-1 (SGPL1) have also been explored in response to shear stress [60,61] and are investigated here using live, cell-laden HEMV to in order validate the model. Interestingly, differential gene regulation occurred within a relatively short time frame (1h or 3h) (Fig. 5) suggesting that perfusion has an earlier effect on cellular dynamics than previously reported [61–63]. The most prominent changes are observed in *SMAD7*, *KLF2* and *SPHK1* with 3.5-, 4.5- and 3.1-fold increases respectively ($p < 0.001$). Conversely, *SMAD6* and *SGPL1* were downregulated 3.8- and 1.7-fold ($p < 0.001$; $p < 0.05$), respectively, after 1h of perfusion. Furthermore, the differential effects observed between SMAD6 and SMAD7 under perfusion assays are noteworthy. Shear stress likely targets the BMP pathway for enhanced expression, observed here as relieved repression; while conversely TGF-β activation is inhibited via SMAD7, indicating TGF-β may not be required by endothelial cells under shear-stress, an observation supported in other work [64]. Also, the slight repression of SGPL1 observed here is consistent with the increases observed in SGPK1, as SGPL1 functions as a negative regulator of SPHK1.

Finally, genes such as EphrinB2 (*EFNB2*) and EphB4 (*EPHB4*) have previously been shown to function as biomarkers capable of differentiating between arterial and venous blood vessels [65–68]. Arterial-derived blood vessels have been shown to express the transmembrane ligand EphrinB2, while venous-derived vessels have been shown to express EphB4, the cognate receptor for EphrinB2. In order to determine if EphrinB2 or EphB4 can be used to distinguish HEMV and MCMV under perfusion, live HEMV or MCMV were exposed to shear stresses for up to 2 h (Fig. 5d–e) and RNA was assessed via quantitative RT-PCR. Expression of EphrinB2 was observed increased 2.3-fold ($p < 0.01$) in MCMV, when compared to static control (0h), while no such upregulation was observed in HEMV under the same perfusion rate. Similarly, in perfused HEMV, EphB4 displayed a more modest, though

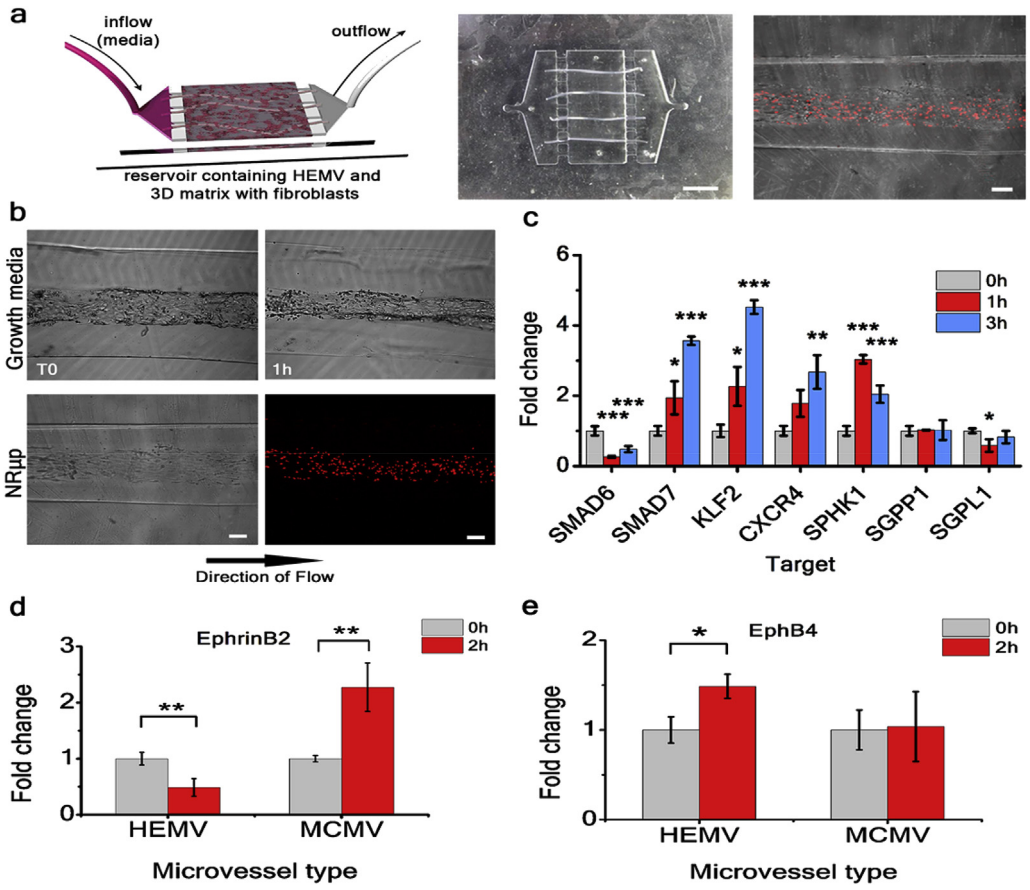

Fig. 5. Microfluidic manifold and modeling shear-stress response. (a) *Left*, diagram of novel microfluidic manifold device; *middle*, HEMV loaded manifold; *right*, transmission/Nile Red microparticles (NRμp, 2 μm O.D.) overlay of HEMV under perfusion. Scale, 1.5 cm and 50 μm, respectively. (b) Live-HEMV were used to perfuse either endothelial growth media or microparticles in a recirculated fashion using separate microvessels at 4 dyn/cm^2. Scale, 50 μm (c) Shear-stress response genes were examined via real-time PCR from growth-media perfused HEMV. Genes with the most differential regulation include the TGF-β members *SMAD6* (downregulated 3.8-fold; $p < 0.001$) and *SMAD7* (upregulated 3.5-fold, $p < 0.001$). Other observed changes included *SPHK1* (upregulated 3.1-fold; $p < 0.001$) and *SGPL1* (downregulated 1.7-fold; $p < 0.05$). *SGPP1* was observed unchanged. (d and e) EphrinB2 or EphrinB4 are biomarkers capable of distinguishing arterial from venous blood vessels, respectively. The effect of perfusion on EphrinB2 and EphB4 gene expression was assessed using either live HEMV or live multi-cell microvessels (MCMV) via real-time PCR. In the arterial-like MCMV, EphrinB2 was observed upregulated 2.3-fold ($p < 0.01$); while EphB4 was upregulated 1.4-fold ($p < 0.03$) in venous-like HMEV in response to growth media perfusion. Statistical analyses shown compare the 2 h perfusion group to static perfusion 0 h control microvessels. Error bars depict standard error of the mean (SEM) of 3 biological replicates.

significant 1.4-fold ($p < 0.03$) increase in response to HEMV perfusion indicating appropriate identification of a venous-like microvessel.

In summary, results obtained from perfusion experiments using the manifold device show that HEMV support perfusion and respond to shear stress, significantly improving upon *in vitro* endothelial networks and acellular microchannel conduits used in other applications. Additionally, the EphrinB2 and EphB4 biomarkers distinguish HEMV from MCMV, thus providing biochemical evidence that fabricated microvessels can exhibit differential responses to the appropriate signaling cue, whether from a growth factor for an integral signaling pathway such as TGF-beta or shear stress in response to perfusion.

4. Conclusions

Technological advances in microfluidics combined with improved biocompatible materials have made microfabrication of human blood vessels a possibility [20–24,52]. Combining a functional vasculature which displays developmental processes to support complex tissue constructs is critical, and many of the developmental process observed in native human blood vessels have been recapitulated using HEMV technology. In summary, biochemical and mechanical analyses illustrate that HEMV support single- or multi-cell attachment and growth; remodel their extracellular matrix by incorporating native human proteins into the vessel wall; remain hollow/porous tubules of the predesigned size and function in a matrix of other cells. In addition, HEMV promote angiogenesis, tubulogenesis and anastomosis together as a single system within a three-dimensional *in vitro* tissue model. Further, perfused HEMV permit the biochemical analyses of HEMV under various flow conditions. When compared to other constructs, such as decellularized vessel scaffolds, HEMV reduce the potential transfer of donor pathogens, are more comparable in size to human venules/arterioles and are easily positioned into a tissue model. Most notably, the extensive neoangiogenesis observed from embedded HEMV and the capacity for long-term storage underscore the versatility that both freshly prepared and cryopreserved HEMV provide, allowing the user to design, create and store the fabricated HEMV for future use. Concerning neoangiogenesis, importantly we find embedded HEMVs self-vascularize their surrounding ECM eliminating the need to fully ‘engineer’ tissue vascularization. Rather, the cells present in the HEMV respond to signaling cues that direct where and to what extent angiogenesis should occur, which is more representative of the native state of vascular development. Finally, other technologies such as 3D

printing, while undoubtedly promising, have yet to produce a human vascularized model that can exhibit long-term viability, extensive angiogenesis, perfusion and blood vessel storage. Thus, HEMV technology provides a level of flexibility and experimental standardization not possible using endothelial spheroid cultures or other microvessel technologies.

Author contributions

F.L., M.D. and A.A. conceived the technology for fabricating microvessels using hydrodynamic focusing. A.A. and S.R. fabricated sheath flow systems and perfusion chambers. K.D., M.D. and A.A. co-designed the research plan. K.D. fabricated microvessels and performed the characterization, angiogenesis and validation experiments. S.R and M.D. performed perfusion simulations. M.D. contributed to the development of the PEG/GelMA materials. K.D. and M.D. co-drafted the paper. All authors discussed the results and edited the manuscript.

Competing financial interests

The authors declare no competing interests.

Acknowledgements

This work was funded by the Naval Research Laboratory/Office of Naval Research MA041-06-41-4639 (A.A.); the Naval Research Laboratory Karle's Fellowship (K.D.) and the Defense Threat Reduction Agency HDTRA1-5-1-7467 (A.A.). The views are those of the authors and do not represent the opinion or policy of the U.S. Navy or U.S. Department of Defense. The intellectual property referenced in this work is owned by the US Navy. Kyle DiVito contributed to this work as an Association for Science and Engineering Education (ASEE) Postdoctoral Fellow. Steven A. Roberts contributed to this work as a Naval Research Enterprise Internship Program participant.

The authors would also like to thank S. Rabbany (Hofstra University) for providing the shear stress related gene targets (SMAD6, SMAD7, KLF2, CXCR4). Also, many thanks to A. Steward (NCSU); as well as S. Walper, K. Turner, E. Goldman and D. Zabetakis (NRL) for aid in qPCR.

Appendix A. Supplementary data

Supplementary data related to this article can be found at http://dx.doi.org/10.1016/j.biomaterials.2017.05.012.

References

[1] B. Derby, Printing and prototyping of tissues and scaffolds, Science 338 (2012) 921–926.
[2] E.S. Lippmann, S.M. Azarin, J.E. Kay, R.A. Nessler, H.K. Wilson, A. Al-Ahmad, et al., Derivation of blood-brain barrier endothelial cells from human pluripotent stem cells, Nat. Biotechnol. 30 (2012) 783–791.
[3] A.S. Mao, D.J. Mooney, Regenerative medicine: current therapies and future directions, Proc. Natl. Acad. Sci. U. S. A. 112 (2015) 14452–14459.
[4] S.G. Rayner, Y. Zheng, Engineered microvessels for the study of human disease, J. Biomech. Eng. (2016) 138.
[5] C.B. Pinnock, E.M. Meier, N.N. Joshi, B. Wu, M.T. Lam, Customizable engineered blood vessels using 3D printed inserts, Methods 99 (2016) 20–27.
[6] L. Gui, B.C. Dash, J. Luo, L. Qin, L. Zhao, K. Yamamoto, et al., Implantable tissue-engineered blood vessels from human induced pluripotent stem cells, Biomaterials 102 (2016) 120–129.
[7] G.A. Truskey, C.E. Fernandez, Tissue-engineered blood vessels as promising tools for testing drug toxicity, Expert Opin. Drug Metab. Toxicol. 11 (2015) 1021–1024.
[8] C.E. Fernandez, H.E. Achneck, W.M. Reichert, G.A. Truskey, Biological and engineering design considerations for vascular tissue engineered blood vessels (TEBVs), Curr. Opin. Chem. Eng. 3 (2014) 83–90.
[9] R. Samuel, L. Daheron, S. Liao, T. Vardam, W.S. Kamoun, A. Batista, et al., Generation of functionally competent and durable engineered blood vessels from human induced pluripotent stem cells, Proc. Natl. Acad. Sci. U. S. A. 110 (2013) 12774–12779.
[10] S. Dimitrievska, C. Cai, A. Weyers, J.L. Balestrini, T. Lin, S. Sundaram, et al., Click-coated, heparinized, decellularized vascular grafts, Acta biomater. 13 (2015) 177–187.
[11] E. Hoch, G.E. Tovar, K. Borchers, Bioprinting of artificial blood vessels: current approaches towards a demanding goal. European journal of cardio-thoracic surgery, Off. J. Eur. Assoc. Cardio-thoracic Surg. 46 (2014) 767–778.
[12] J.S. Choi, Y. Piao, T.S. Seo, Fabrication of a circular PDMS microchannel for constructing a three-dimensional endothelial cell layer, Bioprocess Biosyst. Eng. 36 (2013) 1871–1878.
[13] L.K. Fiddes, N. Raz, S. Srigunapalan, E. Tumarkan, C.A. Simmons, A.R. Wheeler, et al., A circular cross-section PDMS microfluidics system for replication of cardiovascular flow conditions, Biomaterials 31 (2010) 3459–3464.
[14] S.F. Barreto-Ortiz, J. Fradkin, J. Eoh, J. Trivero, M. Davenport, B. Ginn, et al., Fabrication of 3-dimensional multicellular microvascular structures, FASEB J. Off. Publ. Fed. Am. Soc. Exp. Biol. 29 (8) (2015) 3302–3314.
[15] H. Onoe, T. Okitsu, A. Itou, M. Kato-Negishi, R. Gojo, D. Kiriya, et al., Metre-long cell-laden microfibres exhibit tissue morphologies and functions, Nat. Mater. 12 (2013) 584–590.
[16] H.W. Kang, S.J. Lee, I.K. Ko, C. Kengla, J.J. Yoo, A.A. Atala, 3D bioprinting system to produce human-scale tissue constructs with structural integrity, Nat. Biotechnol. 34 (2016) 312–319.
[17] Y.S. Zhang, A. Arneri, S. Bersini, S.R. Shin, K. Zhu, Z. Goli-Malekabadi, et al., Bioprinting 3D microfibrous scaffolds for engineering endothelialized myocardium and heart-on-a-chip, Biomaterials 110 (2016) 45–59.
[18] J.S. Miller, K.R. Stevens, M.T. Yang, B.M. Baker, D.H. Nguyen, D.M. Cohen, et al., Rapid casting of patterned vascular networks for perfusable engineered three-dimensional tissues, Nat. Mater. 11 (2012) 768–774.
[19] S.P. Herbert, D.Y. Stainier, Molecular control of endothelial cell behaviour during blood vessel morphogenesis, Nat. Rev. Mol. Cell Biol. 12 (2011) 551–564.
[20] M.A. Daniele, A.A. Adams, J. Naciri, S.H. North, F.S. Ligler, Interpenetrating networks based on gelatin methacrylamide and PEG formed using concurrent thiol click chemistries for hydrogel tissue engineering scaffolds, Biomaterials 35 (2014) 1845–1856.
[21] M.A. Daniele, D.A. Boyd, A.A. Adams, F.S. Ligler, Microfluidic strategies for design and assembly of microfibers and nanofibers with tissue engineering and regenerative medicine applications, Adv. Healthc. Mater 4 (2015) 11–28.
[22] M.A. Daniele, K. Radom, F.S. Ligler, A.A. Adams, Microfluidic fabrication of multiaxial microvessels via hydrodynamic shaping, RSC Adv. 4 (2014) 23440–23446.
[23] M. Nikkhah, N. Eshak, P. Zorlutuna, N. Annabi, M. Castello, K. Kim, et al., Directed endothelial cell morphogenesis in micropatterned gelatin methacrylate hydrogels, Biomaterials 33 (2012) 9009–9018.
[24] H. Shin, B.D. Olsen, A. Khademhosseini, The mechanical properties and cytotoxicity of cell-laden double-network hydrogels based on photocrosslinkable gelatin and gellan gum biomacromolecules, Biomaterials 33 (2012) 3143–3152.
[25] K.A. DiVito, C.M. Simbulan-Rosenthal, Y.S. Chen, V.A. Trabosh, D.S. Rosenthal, Id2, Id3 and Id4 overcome a Smad7-mediated block in tumorigenesis, generating TGF-beta-independent melanoma, Carcinogenesis 35 (2014) 951–958.
[26] K.A. DiVito, V.A. Trabosh, Y.S. Chen, C.M. Simbulan-Rosenthal, D.S. Rosenthal, Inhibitor of differentiation-4 (Id4) stimulates pigmentation in melanoma leading to histiocyte infiltration, Exp. Dermatol. 24 (2015) 101–107.
[27] R. Costa-Almeida, M. Gomez-Lazaro, C. Ramalho, P.L. Granja, R. Soares, S.G. Guerreiro, Fibroblast-endothelial partners for vascularization strategies in tissue engineering, Tissue Eng. Part A 21 (2015) 1055–1065.
[28] S.G. Guerreiro, M.J. Oliveira, M.A. Barbosa, R. Soares, P.L. Granja, Neonatal human dermal fibroblasts immobilized in RGD-alginate induce angiogenesis, Cell Transplant. 23 (2014) 945–957.
[29] X. Wang, S. Abraham, J.A. McKenzie, N. Jeffs, M. Swire, V.B. Tripathi, et al., LRG1 promotes angiogenesis by modulating endothelial TGF-beta signalling, Nature 499 (2013) 306–311.
[30] G. Bergers, S. Song, The role of pericytes in blood-vessel formation and maintenance, Neuro-oncology 7 (2005) 452–464.
[31] N. Kalinina, D. Kharlampieva, M. Loguinova, I. Butenko, O. Pobeguts, A. Efimenko, et al., Characterization of secretomes provides evidence for adipose-derived mesenchymal stromal cells subtypes, Stem Cell Res. Ther. 6 (2015) 221.
[32] J. Wang, A. Svendsen, J. Kmiecik, H. Immervoll, K.O. Skaftnesmo, J. Planaguma, et al., Targeting the NG2/CSPG4 proteoglycan retards tumour growth and angiogenesis in preclinical models of GBM and melanoma, PloS One 6 (2011) e23062.
[33] S. Yadavilli, E.I. Hwang, R.J. Packer, J. Nazarian, The role of NG2 proteoglycan in glioma, Transl. Oncol. 9 (2016) 57–63.
[34] P.M. Hinderliter, K.R. Minard, G. Orr, W.B. Chrisler, B.D. Thrall, J.G. Pounds, et al., ISDD: a computational model of particle sedimentation, diffusion and target cell dosimetry for in vitro toxicity studies, Part. fibre Toxicol. 7 (2010) 36.
[35] K.A. DiVito, M.A. Daniele, S.A. Roberts, F.S. Liger, A.A. Adams, Characterizing microfabricated human blood vessels created via hydrodynamic focusing, Data Brief (2017) (in press).

[36] F.S. Ligler, A.A. Adams, M.A. Daniele, in: U. Navy (Ed.), Micro Blood Vessels and Tissue Ducts, 2015. United States.
[37] D.R.H.P. Mott, F.S. Ligler, S. Fertig, A. Bobrokowski, in: U. Navy (Ed.), Sheath Flow Device and Method, 2015. United States.
[38] A. Dellavalle, M. Sampaolesi, R. Tonlorenzi, E. Tagliafico, B. Sacchetti, L. Perani, et al., Pericytes of human skeletal muscle are myogenic precursors distinct from satellite cells, Nat. Cell Biol. 9 (2007) 255–267.
[39] A. Armulik, A. Abramsson, C. Betsholtz, Endothelial/pericyte interactions, Circ. Res. 97 (2005) 512–523.
[40] G.D. Collett, A.E. Canfield, Angiogenesis and pericytes in the initiation of ectopic calcification, Circ. Res. 96 (2005) 930–938.
[41] V. Nehls, D. Drenckhahn, The versatility of microvascular pericytes: from mesenchyme to smooth muscle? Histochemistry 99 (1993) 1–12.
[42] S. Ortiz-Urda, J. Garcia, C.L. Green, L. Chen, Q. Lin, D.P. Veitch, et al., Type VII collagen is required for Ras-driven human epidermal tumorigenesis, Science 307 (2005) 1773–1776.
[43] D. Vestweber, How leukocytes cross the vascular endothelium, Nat. Rev. Immunol. 15 (2015) 692–704.
[44] R.B. Huang, O. Eniola-Adefeso, Shear stress modulation of IL-1beta-induced E-selectin expression in human endothelial cells, PloS One 7 (2012) e31874.
[45] Y.C. Lim, K. Snapp, G.S. Kansas, R. Camphausen, H. Ding, F.W. Luscinskas, Important contributions of P-selectin glycoprotein ligand-1-mediated secondary capture to human monocyte adhesion to P-selectin, E-selectin, and TNF-alpha-activated endothelium under flow in vitro, J. Immunol. 161 (1998) 2501–2508.
[46] E. Prugberger, Hilar lymph node swelling as a reaction to BCG-hypersensitivity (author's transl), Z. Erkrank. Atmungsorgane 147 (1977) 51–56.
[47] J. Shen, Schrieber L. SS TT, N.J. King, Early E-selectin, VCAM-1, ICAM-1, and late major histocompatibility complex antigen induction on human endothelial cells by flavivirus and comodulation of adhesion molecule expression by immune cytokines, J. virol. 71 (1997) 9323–9332.
[48] Y. Sugama, C. Tiruppathi, K. Offakidevi, T.T. Andersen, J.W. Fenton 2nd, A.B. Malik, Thrombin-induced expression of endothelial P-selectin and intercellular adhesion molecule-1: a mechanism for stabilizing neutrophil adhesion, J. Cell Biol. 119 (1992) 935–944.
[49] J. Massague, TGFbeta signalling in context, Nat. Rev. Mol. Cell Biol. 13 (2012) 616–630.
[50] S.M. Ehsan, S.C. George, Nonsteady state oxygen transport in engineered tissue: implications for design, Tissue Eng. Part A 19 (2013) 1433–1442.
[51] L. Tian, S.C. George, Biomaterials to prevascularize engineered tissues, J. Cardiovasc. Transl. Res. 4 (2011) 685–698.
[52] S.A. Roberts, K.A. DiVito, F.S. Ligler, A.A. Adams, M.A. Daniele, Microvessel manifold for perfusion and media exchange in three-dimensional cell cultures, Biomicrofluidics 10 (2016) 054109.
[53] A. Lenard, S. Daetwyler, C. Betz, E. Ellertsdottir, H.G. Belting, J. Huisken, et al., Endothelial cell self-fusion during vascular pruning, PLoS Biol. 13 (2015) e1002126.
[54] A. Lenard, E. Ellertsdottir, L. Herwig, A. Krudewig, L. Sauteur, H.G. Belting, et al., In vivo analysis reveals a highly stereotypic morphogenetic pathway of vascular anastomosis, Dev. Cell 25 (2013) 492–506.
[55] M.A. Daniele, S.A. Roberts, F.S. Ligler, A.A. Adams, in: USPTO (Ed.), Modular Microtube Network for Vascularized Organ-On-A-Chip Models, 2016.
[56] Y.X. Qi, J. Jiang, X.H. Jiang, X.D. Wang, S.Y. Ji, Y. Han, et al., PDGF-BB and TGF-{beta}1 on cross-talk between endothelial and smooth muscle cells in vascular remodeling induced by low shear stress, Proc. Natl. Acad. Sci. U. S. A. 108 (2011) 1908–1913.
[57] K.A. DiVito, V.A. Trabosh, Y.S. Chen, Y. Chen, C. Albanese, D. Javelaud, et al., Smad7 restricts melanoma invasion by restoring N-cadherin expression and establishing heterotypic cell-cell interactions in vivo, Pigment Cell & melanoma Res. 23 (2010) 795–808.
[58] A. Hanyu, Y. Ishidou, T. Ebisawa, T. Shimanuki, T. Imamura, K. Miyazono, The N domain of Smad7 is essential for specific inhibition of transforming growth factor-beta signaling, J. Cell Biol. 155 (2001) 1017–1027.
[59] T. Imamura, M. Takase, A. Nishihara, E. Oeda, J. Hanai, M. Kawabata, et al., Smad6 inhibits signalling by the TGF-beta superfamily, Nature 389 (1997) 622–626.
[60] R.J. Dekker, S. van Soest, R.D. Fontijn, S. Salamanca, P.G. de Groot, E. VanBavel, et al., Prolonged fluid shear stress induces a distinct set of endothelial cell genes, most specifically lung Kruppel-like factor (KLF2), Blood 100 (2002) 1689–1698.
[61] K. Venkataraman, Y.M. Lee, J. Michaud, S. Thangada, Y. Ai, H.L. Bonkovsky, et al., Vascular endothelium as a contributor of plasma sphingosine 1-phosphate, Circ. Res. 102 (2008) 669–676.
[62] A.D. Egorova, K. Van der Heiden, S. Van de Pas, P. Vennemann, C. Poelma, M.C. DeRuiter, et al., Tgfbeta/Alk5 signaling is required for shear stress induced klf2 expression in embryonic endothelial cells. Developmental dynamics, Off. Publ. Am. Assoc. Anatomists 240 (2011) 1670–1680.
[63] B. Jung, H. Obinata, S. Galvani, K. Mendelson, B.S. Ding, A. Skoura, et al., Flow-regulated endothelial S1P receptor-1 signaling sustains vascular development, Dev. Cell 23 (2012) 600–610.
[64] J. Zhou, P.L. Lee, C.I. Lee, S.Y. Wei, S.H. Lim, T.E. Lin, et al., BMP receptor-integrin interaction mediates responses of vascular endothelial Smad1/5 and proliferation to disturbed flow, J. Thromb. Haemost. 11 (2013) 741–755.
[65] N.W. Gale, P. Baluk, L. Pan, M. Kwan, J. Holash, T.M. DeChiara, et al., Ephrin-B2 selectively marks arterial vessels and neovascularization sites in the adult, with expression in both endothelial and smooth-muscle cells, Dev. Biol. 230 (2001) 151–160.
[66] A. Sivarapatna, M. Ghaedi, A.V. Le, J.J. Mendez, Y. Qyang, L.E. Niklason, Arterial specification of endothelial cells derived from human induced pluripotent stem cells in a biomimetic flow bioreactor, Biomaterials 53 (2015) 621–633.
[67] F. le Noble, D. Moyon, L. Pardanaud, L. Yuan, V. Djonov, R. Matthijsen, et al., Flow regulates arterial-venous differentiation in the chick embryo yolk sac, Development 131 (2004) 361–375.
[68] H.U. Wang, Z.F. Chen, D.J. Anderson, Molecular distinction and angiogenic interaction between embryonic arteries and veins revealed by ephrin-B2 and its receptor Eph-B4, Cell 93 (1998) 741–753.